Chapter 16
A Novel Kinematic Model for Rough Terrain Robots

Joseph Auchter, Carl A. Moore, and Ashitava Ghosal

Abstract We describe in detail a novel kinematic simulation of a three-wheeled mobile robot moving on extremely uneven terrain. The purpose of this simulation is to test a new concept, called Passive Variable Camber (PVC), for reducing undesirable wheel slip. PVC adds an extra degree of freedom at each wheel/platform joint, thereby allowing the wheel to tilt laterally. This extra motion allows the vehicle to better adapt to uneven terrain and reduces wheel slip, which is harmful to vehicle efficiency and performance.

In order to precisely model the way that three dimensional wheels roll over uneven ground, we adapt concepts developed for modeling dextrous robot manipulators. The resulting equations can tell us the instantaneous mobility (number of degrees of freedom) of the robot/ground system. We also showed a way of specifying joint velocity inputs which are compatible with system constraints. Our modeling technique is adaptable to vehicles of arbitrary number of wheels and joints.

Based on our simulation results, PVC has the potential to greatly improve the motion performance of wheeled mobile robots or any wheeled vehicle which moves outdoors on rough terrain by reducing wheel slip.

Keywords Kinematics · Mobile robots · Uneven terrain · Dextrous manipulation

16.1 Introduction

Wheeled mobile robots (WMRs) were first developed for indoor use. As such, traditional kinematic models reflect assumptions that can be made about the structured

J. Auchter (✉) and C.A. Moore
Department of Mechanical Engineering, FAMU/FSU College of Engineering in Tallahassee, Florida, USA
e-mail: auchtjo@eng.fsu.edu

A. Ghosal
Department of Mechanical Engineering, Indian Institute of Science in Bangalore, India

S.-I. Ao et al. (eds.), *Advances in Computational Algorithms and Data Analysis,*
Lecture Notes in Electrical Engineering 14,

environment in which the robot operates [1]. For example, the robot is assumed to move on a planar surface. The wheels are modeled as thin disks and the velocity of each wheel center, v, in terms of its angular speed ω is calculated as $v = \omega R$. As a result of these assumptions, the non-holonomic constraints of wheel rolling without slip at the wheel/ground contacts are simple trigonometric relationships.

Recently there have been many attempts to extend the operating range of WMRs to outdoor environments [2–4]. As a result the kinematic modeling process becomes very complex, mainly because the robot is now moving in a three-dimensional world instead of a two-dimensional one. On uneven terrain the contact point can vary along the surface of the wheel in both lateral and longitudinal directions. Therefore it no longer justifiable to model the wheel as a thin disk. Furthremore, the non-holonomic constraints can no longer be determined by simple geometry. Despite these difficulties, kinematic modeling is a crucial process since it is used for control and path planning [5, 6] and as a stepping stone to a dynamic model.

16.1.1 Previous Work

There have been several recent efforts to model the kinematic motion of WMRs on uneven terrains. However, none of them provide a complete model for the motion of the wheel rolling over the uneven ground. Capturing this motion precisely is of utmost importance when studying wheel slip, power efficiency, climbing ability, and path planning for outdoor robots.

In reference [7], the authors provide a detailed kinematic model for the Rocky 7 Mars rover, but assume a 2-D wheel and do not provide a model of how the contact point moves along the surface of the wheel as it rolls on an uneven ground. In the reference [8], the authors develop a similar kinematic model for their CEDRA robot. However, they assume that certain characteristics of the wheel motion on the terrain are known without providing any equations describing the motion. The kinematic model in reference [9] places a coordinate frame at the wheel/ground contact point, but no explanation is provided as to where the contact point is or how the motion is influenced by the terrain shape. Grand and co-workers [10] perform a velocity analysis on their hybrid wheel-legged robot Hylos. They identify the contact point for each wheel and an associated frame, but make no mention of how these frames evolve as the vehicle moves. Sreenivasan and Nanua [11] explore first- and second-order kinematic characteristics of wheeled vehicles on uneven terrain in order to determine vehicle mobility. For general terrains, their method is inefficient and involves manual determination of free joint rates to avoid interdependencies.

16.1.2 Kinematic Slip

The unstructured outdoor environment can cause unexpected problems for wheeled mobile robots. In addition to dynamic slippage due to terrain deformation or

insufficient friction, a WMR is affected by kinematic slip [4, 12, 13]. Kinematic slip occurs when there is no instantaneous axis of rotation compatible with all of the robot's wheels. For automobiles this can lead to tire scrubbing and is generally avoided using Ackermann steering geometry. This works properly only on flat ground, however. On uneven terrain kinematic slip occurs generally with a standard vehicle since the location of the wheel/ground contact point varies laterally and longitudinally over the wheel surface due to the terrain shape and robot configuration.

Wheel slip causes several problems: first, power is wasted [4, 12], and second, wheel slip reduces the ability of the robot to self-localize because position estimates from wheel encoder data accumulate unbounded error over time [14]. Researchers have reported that reducing slip improves the climbing performance and accuracy of the odometry for a six-wheeled off-road rover [15]. Accurate kinematic models are needed to test robot designs which will potentially reduce this costly kinematic slip. In reference [11], the authors used screw theory to explore the phenomenon of kinematic slip in wheeled vehicle systems moving on uneven terrain. Their analysis showed that kinematic slip can be avoided if the distance between the wheel/ground contact points is allowed to vary for two wheels joined on an axle. The authors of that work suggest the use of a Variable Length Axle (VLA) with a prismatic joint to achieve the necessary motion. The VLA is difficult to implement because it requires a complex wheel axle design.

As a more practical alternative to the VLA, the authors in reference [12] introduced the idea of adding an extra degree of freedom (DOF) at the wheel/axle joint, allowing the wheel to tilt laterally relative to the axle. This new capability, herein named Passive Variable Camber (PVC), permits the distance between the wheel/ground contact points to change without any prismatic joints. On a real vehicle the PVC joints would be actuated by lateral forces at the wheel/ground interface arising from interactions between the two surfaces; therefore, the joint would be "passive" (requiring no extra energy expenditure by the robot). Figure 16.1 shows an example of an axle and two wheels equipped with PVC.

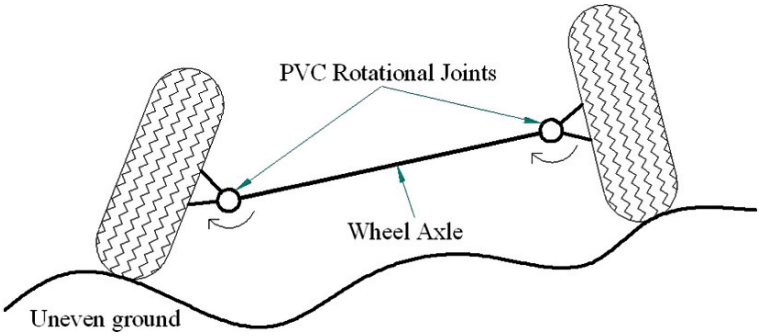

Fig. 16.1 Two tires on uneven ground attached to an axle equipped with Passive Variable Camber. The axis of rotation of each PVC joint is perpendicular to the page

16.1.3 Contribution of this Work

Traditional methods are not suitable for kinematic modeling of outdoor WMRs due to the complex nature of the terrain/robot system. More recent efforts to model outdoor vehicle motion lack convincing descriptions of how a realistic wheel rolls over an arbitrary uneven terrain.

This paper describes in detail a novel kinematic simulation of a three-wheeled mobile robot equipped with Passive Variable Camber and moving on uneven terrain. In order to precisely model the way that three dimensional wheels roll over uneven ground, we adapted concepts developed for modeling dextrous robot manipulators. In the reference [12] the authors began this task by using dextrous manipulation contact kinematics to model how a torus-shaped wheel rolls over an arbitrarily-shaped smooth terrain. In their WMR model they introduced an extra degree of freedom at the wheel which allowed for lateral tilting in order to prevent kinematic slip. In this paper we extend that work by completing the analogy between dextrous manipulators and wheeled vehicles using additional equations which give more insight into the structure of the system, including the number of degrees of freedom and the interdependencies among joint rates.

To the best of our knowledge, the union of the worlds of WMR modeling and dextrous manipulator modeling is novel and does not suffer from many of the assumptions inherent in other modeling techniques. Our method provides a concise and manageable description of the kinematics and is easily adaptable to other vehicle designs of arbitrary complexity.

The purpose of our simulation is to verify that a WMR equipped with PVC can traverse uneven terrain without kinematic slip. Based on the simulation results, PVC has the potential to greatly improve the motion performance of wheeled mobile robots, or any wheeled vehicle which moves outdoors on rough terrain.

16.2 Analogy Between WMRs and Dextrous Manipulators

In this work a kinematic model of the WMR/ground system is developed using techniques from the field of dextrous manipulation. This is extremely useful for the WMR community because the kinematics of dextrous manipulation provide an ideal description of the way wheels roll over uneven terrain. To our knowledge, the analogy between a robotic hand manipulating an object and a WMR traversing a three-dimensional terrain had never been made before the work of Chakraborty and Ghosal [12]. A WMR in contact with uneven ground is analogous to a multi-fingered robotic “hand” (the WMR) grasping an “object” (the ground). Table 16.1 summarizes the analogies between robotic hands and WMRs.

Table 16.1 Relationships between manipulators and WMRs

Manipulators	Mobile robots
Multi-fingered hand	Wheeled mobile robot
Grasped object	Ground
Fingers	Wheels
Palm	Robot platform

16.3 Off-Road Wheeled Mobile Robot Kinematic Model

In this paper we model a three-wheeled mobile robot (one front and two rear wheels). The front wheel is steerable and the two rear wheels have Passive Variable Camber (PVC) joints. The wheels are torus-shaped, which is more realistic than the typical thin-disk model. We adapt techniques from the field of dextrous manipulator modeling to show that the PVC-equipped wheeled mobile robot is able to negotiate extreme terrains without kinematic wheel slip. This is desirable because rolling motion is more controlled than sliding motion. Our simulation and evaluation process involves the following steps:

1. Write kinematic differential equations which describe the system, including the wheel/ground contact
2. Constrain the wheels to roll by suitable modification of the contact equations
3. Run simulations on various types of uneven terrain and
4. Monitor the level of constraint violation

As will be shown, the rolling constraints are well-satisfied for all of the simulations that we have attempted. This means that PVC has the potential to dramatically reduce undesirable wheel slip for a real vehicle operating on rough terrains.

16.3.1 Wheel/Ground Contact Model

At the heart of our novel WMR modeling concept is the use of dextrous manipulation equations to describe how the wheel rolls over the ground surface in response to the robot's velocity inputs. These equations are powerful because they were originally formulated to show how a robotic finger rolls/slides over an object of any shape, provided that both finger and object are smooth surfaces. Therefore, the equations can easily be applied to the special case of smooth wheels rolling over an uneven ground.

Montana [16] was the first to develop kinematic contact equations which describe how two arbitrarily-shaped smooth surfaces roll/slide against each other. In our case the two surfaces are the wheel and ground. In this section we will develop the tools that we need in order to make use of the contact equations. For a good overview of dextrous manipulation and the associated mathematics, see [17].

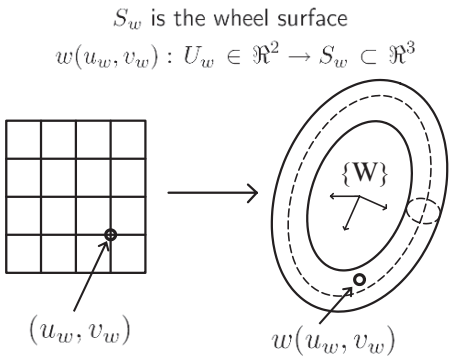

Fig. 16.2 Wheel surface parameterization

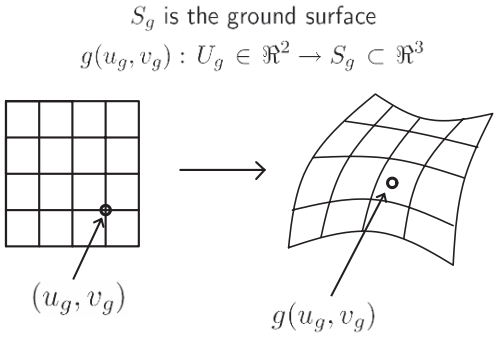

Fig. 16.3 Ground surface parameterization

Figures 16.2 and 16.3 show the surface parameterizations that we will use. The surface of the wheel is parameterized relative to its frame $\{W\}$ by the right-handed orthogonal coordinate chart:

$$w(u,v):\ U\ \in\ \Re^2 \rightarrow S_w\ \subset\ \Re^3$$

In other words, specifying two parameters u_i and v_i will locate a unique point on the surface of wheel i. Similarly, the ground surface is parameterized relative to its frame $\{G\}$ by the chart $g(x,y)$, meaning that any parameters x and y will locate a unique point $(x,y,g(x,y))$ or (x,y,z) on the ground surface.

Montana's equations describe the motion of the point of contact across the surfaces in response to a relative motion between the wheel and the ground. This motion has five degrees of freedom (DOFs), the one constraint being that there be no translational component of motion along their common surface normal and contact is maintained. These five DOFs have the following interpretation: two DOFs each for the position of the contact point on the two surfaces (wheel and ground), and one DOF for rotation about the surface normal. The parameters that describe these five DOFs for wheel i are

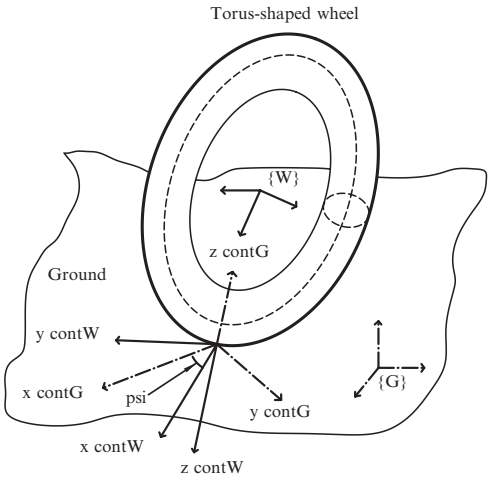

Fig. 16.4 Coordinate frames of the wheel and ground

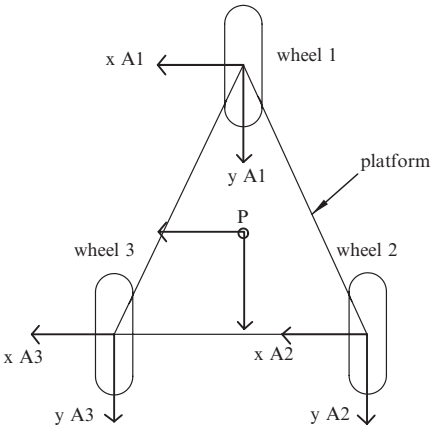

Fig. 16.5 Coordinate frames of the robot platform

$$\eta_i = [u_i \; v_i \; x_i \; y_i \; \psi_i]^T, \quad i = 1,2,3$$

where ψ_i is the angle of rotation about the common surface normal. They are grouped for all three wheels as: $\eta = [\eta_1^T \; \eta_2^T \; \eta_3^T]^T$.

Figures 16.4 and 16.5 show the coordinate frames which are used to develop the WMR kinematic model. The frames in Fig. 16.4 follow the conventions of Montana [16, 18] and Murray et al. [17].

In the above figures frame $\{G\}$ is the ground inertial reference frame and frame $\{contG_i\}$ is the ground contact frame for wheel i. The z-axis of $\{contG_i\}$ is the outward normal to the ground surface at the contact point. Frame $\{P\}$ is the robot platform reference frame, $\{A_i\}$ is the frame at the point of attachment of the wheel i to the platform, and $\{W_i\}$ is the reference frame of wheel i. The frame $\{contW_i\}$ is the contact frame relative to wheel i. Its z-axis is the outward pointing normal

from the torus-shaped wheel, which is collinear with the z-axis of $\{contG_i\}$. The variable ψ_i (described above) is the angle between the x-axes of frames $\{contG_i\}$ and $\{contW_i\}$. Note that the origin of $\{contG_i\}$ is the point $g(x_i, y_i)$, and the origin of $\{contW_i\}$ is the point $f(u_i, v_i)$ as described above.

Also important are the velocities of the wheel relative to the ground:

$$^{contW}V_{GW} = V_c = [v_x \; v_y \; v_z \; \omega_x \; \omega_y \; \omega_z]^T \tag{16.1}$$

The leading superscript indicates that the vector is resolved in the $\{contW\}$ frame. The subscript GW means that these velocities are of the $\{W\}$ frame relative to the $\{G\}$ frame.

The purpose of our simulation is to show that Passive Variable Camber (PVC) can reduce wheel slip and allow the vehicle to move with a controlled rolling motion over uneven terrains. For our model, this means that the $\{contW\}$ and $\{contG\}$) frames do not translate relative to each other and only relative rolling is permitted. Mathematically, these conditions are expressed as constraints on the velocities V_c:

$$\tilde{V_c} = \bar{B} \; V_c \tag{16.2}$$

where $\bar{B} = [0_{3\times3} \; I_{3\times3}]$. $\tilde{V_c}$, a subset of V_c (from (16.1)), are called the allowable contact velocities. For a wheel rolling without slip $\tilde{V_c} = [\omega_x \; \omega_y \; \omega_z]^T$.

16.3.1.1 Kinematic Contact Equations

We are now ready to introduce the contact equations. In terms of the metric (M), curvature (K) and torsion (T) forms, the equations for rolling contact are [16]:

$$\begin{aligned} (\dot{u}, \dot{v})^T &= M_w^{-1} \left(K_w + K^*\right)^{-1} (-\omega_y, \omega_x)^T \\ (\dot{x}, \dot{y})^T &= M_g^{-1} R_\psi \left(K_w + K^*\right)^{-1} (-\omega_y, \omega_x)^T \\ \dot{\psi} &= \omega_z + T_w M_w (\dot{u}, \dot{v})^T + T_g M_g (\dot{x}, \dot{y})^T . \end{aligned} \tag{16.3}$$

where subscript w indicates the wheel and g indicates the ground. The inputs to these equations are the allowable wheel contact velocities $\tilde{V_c}$, and the outputs are $\dot{\eta}$, so we abbreviate the equations by:

$$\dot{\eta} = [CK] \; \tilde{V_c}, \tag{16.4}$$

where $[CK]$ stands for "Contact Kinematics". These are the non-holonomic constraints of the robot/ground system by which rolling contact is enforced. During the simulation if these equations are satisfied then the vehicle is moving without slip.

16.3.2 Wheeled Mobile Robot Kinematic Model

In this section we develop the kinematic model of the three-wheeled mobile robot, making use of the contact equations from the previous section to model the

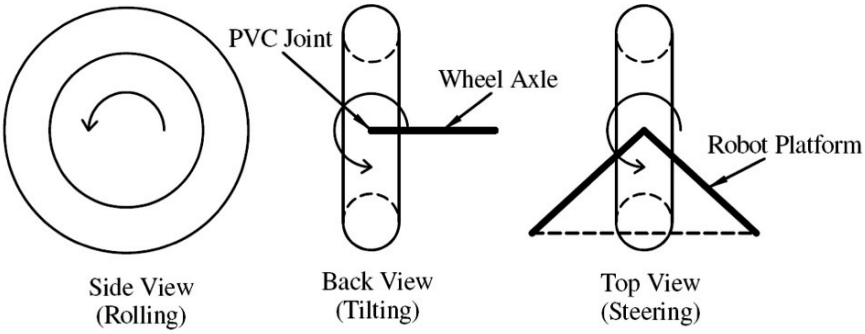

Fig. 16.6 Robot wheel joint velocities

wheel/ground contacts. The inputs and outputs for the forward kinematics are desired wheel and joint velocities $\dot{\theta}$ and position and velocity of robot platform, respectively.

16.3.2.1 Robot Joint Velocities

The vector of joint velocities is:

$$\dot{\theta} = \left[\dot{\phi}_1 \;\; \dot{\alpha}_1 \;\; \dot{\gamma}_2 \;\; \dot{\alpha}_2 \;\; \dot{\gamma}_3 \;\; \dot{\alpha}_3\right]^T$$

where $\dot{\alpha}_i$ is the driving rate of wheel i, $\dot{\phi}_1$ is the steering rate of wheel 1, $\dot{\gamma}_i$ is the rate of tilt of the wheel about the PVC joint of wheel i (for $i = 2,3$). Figure 16.6 graphically illustrates these variables.

16.3.2.2 Choice of Inputs $\dot{\theta}$

The inputs to our forward kinematics simulation are $\dot{\theta}$, the joint velocities (steering rate, driving rate, and PVC tilting rate). Because the robot/ground system has complex non-holonomic constraints (Eq. (16.3)) which depend on the terrain geometry, we cannot choose these inputs arbitrarily: they are interrelated by the structure of the system. In this section we adapt dextrous manipulator equations developed by Han and Trinkle [19] in order to get more insight as to how the joint velocities of our system relate to one another. This will ultimately allow us to calculate $\dot{\theta}$ velocities which are as close as possible (in the least squares sense) to a set of desired velocities.

For the forward kinematics simulation we are interested in calculating the velocities of the robot platform frame $\{P\}$ relative to the ground inertial frame $\{G\}$, which we will call V_{PG}. Following Han and Trinkle [19], we group the platform/ground

relative velocities V_{PG} and contact velocities $\tilde{V}_c$ (see Eq. (16.1)) together in $V_{GC} = \left[V_{PG}^T \; \tilde{V}_c^T \right]^T$. Jacobian matrices can be formed such that:

$$J_{GC} \; V_{GC} = J_R \; \dot{\theta}. \tag{16.5}$$

Equation (16.5) are constraints which relate the joint velocities $\dot{\theta}$ to the relative ground/platform and contact velocities V_{GC}. In the general case neither J_{GC} nor J_R are square and thus are not invertible.

Because of the constraints (16.5), we cannot freely choose our inputs $\dot{\theta}$. However, we can calculate inputs consistent with (16.5) which are as close as possible (in the least-squares sense) to a vector of desired inputs. This is done as follows. The QR decomposition [20] of matrix J_{GC} is:

$$J_{GC} = Q \, R. \tag{16.6}$$

Let r denote $rank(J_{GC})$ and c be the number of columns of J_{GC}. Split Q into $[Q_1 \; Q_2]$, where $Q_2 \in \Re^{c \times (c-r)}$. [The matrix] Q_2 forms a orthonormal basis for the null space of J_{GC}^T, meaning $J_{GC}^T \; Q_2 = 0$ or $Q_2^T \; J_{GC} = 0$. Pre-multiplying both sides of (16.5) by Q_2^T yields $Q_2^T \; J_{GC} \; V_{GC} = Q_2^T \; J_R \; \dot{\theta}$, or

$$Q_2^T \; J_R \; \dot{\theta} = 0. \tag{16.7}$$

Equation (16.7) is a set of constraint equations for the inputs $\dot{\theta}$. To make use of these equations, let $C_\theta = (Q_2^T \; J_R) \in \Re^{p \times q}$ where $p = rank(C_\theta)$. The QR decomposition of C_θ^T is:

$$C_\theta^T = [Q_{C1} \; Q_{C2}] \; R_C,$$

where $Q_{C2} \in \Re^{q \times p}$. Then $C_\theta \; Q_{C2} = 0$, meaning Q_{C2} is an orthonormal basis for the null space of C_θ. At this point, we can choose independent generalized velocity inputs $\dot{\theta}_g$ such that

$$\dot{\theta} = Q_{C2} \; \dot{\theta}_g. \tag{16.8}$$

However, since neither C_θ nor Q_{C2} are unique and both change as the robot configuration changes, the generalized inputs $\dot{\theta}_g$ likely have no physical interpretation and their relationship with the actual joint velocities $\dot{\theta}$ is unclear.

Since (16.8) is of limited use, we take another step. We want our actual joint velocities $\dot{\theta}$ to match some desired joint velocities $\dot{\theta}_d$, or $\dot{\theta} \approx \dot{\theta}_d$. Combining this with (16.8), we have:

$$Q_{C2} \; \dot{\theta}_g \approx \dot{\theta}_d.$$

To get as close as possible in the least squares sense to $\dot{\theta}_d$, we use the pseudo-inverse [21] of Q_{C2}:

$$\dot{\theta}_g = Q_{C2}^+ \; \dot{\theta}_d = (Q_{C2}^T Q_{C2})^{-1} Q_{C2}^T \; \dot{\theta}_d. \tag{16.9}$$

Since the columns of Q_{C2} are orthonormal, Q_{C2}^{+} reduces to Q_{C2}^{T}. Noticing that $\dot{\theta} = Q_{C2}\,\dot{\theta}_g$, we can pre-multiply both sides of (16.9) by Q_{C2} to get $Q_{C2}\dot{\theta}_g = Q_{C2}Q_{C2}^{T}\dot{\theta}_d$, or

$$\dot{\theta} = Q_{C2}Q_{C2}^{T}\dot{\theta}_d = J_{in}\dot{\theta}_d. \tag{16.10}$$

The matrix J_{in} can be thought of as a transformation that takes the desired velocities $\dot{\theta}_d$, which can be arbitrary, and transforms them such that $\dot{\theta}$ satisfy the constraints (16.5) while remaining as close as possible to $\dot{\theta}_d$.

Equation (16.10) is a highly useful result for our simulation. First, it eliminates the need to deal with independent generalized velocities $\dot{\theta}_g$, which have no physical meaning. We can instead directly specify a desired set of joint velocity inputs $\dot{\theta}_d$ and get a set of actual inputs $\dot{\theta}$ which satisfies the constraints (16.5) of the robot/ground system. Second, $\dot{\theta}$ is guaranteed to be as close as possible to $\dot{\theta}_d$ in the least squares sense. Third, (16.10) gives us control over the type of motion we want: for instance, if we want a motion trajectory that minimizes the PVC joint angles $\gamma_{2,3}$ then we set $\dot{\gamma}_{2d} = \dot{\gamma}_{3d} = 0$. The actual γ values will then remain as close to 0 as the system constraints permit, given the desired steering and driving inputs.

16.3.2.3 System Degrees of Freedom

The constraint equation (16.5) and Eq. (16.8) are further useful because they provide a way to determine the number of degrees of freedom (DOFs) of the complex robot/ground system. The size of matrix Q_{C2} explicitly tells us the number of system DOFs. For example, for our system Q_{C2} is 6×3, meaning three generalized inputs and therefore three degrees of freedom. Note that this does not mean we can choose *any* three inputs from $\dot{\theta}$; we can however arbitrarily choose the generalized inputs $\dot{\theta}_g$ and therefore can make use of Eq. (16.10). Also note that the size of Q_{C2} depends on the rank of the original Jacobian matrix J_{GC}. Since J_{GC} is a function of the system configuration, its rank might change for certain singular configurations and therefore the instantaneous number of DOFs would change. In our simulations, however, we have not encountered such a situation.

16.3.3 Holonomic Constraints and Stabilization

The robot/ground system is modeled as a hybrid series-parallel mechanism. Each wheel is itself a kinematic chain between the platform and the ground, and there are three such chains in parallel. Figure 16.7 illustrates the idea. Three chains of coordinate transformations each start at frame $\{G\}$ and end at frame $\{P\}$.

The holonomic *closure constraints* (as opposed to the non-holonomic rolling constraints) for the parallel mechanism specify that each kinematic chain must end at the same frame (in this case, $\{P\}$) [17]. Let T_{AB} be the 4×4 homogeneous rigid body transform between frames A and B. Then the closure constraints for the

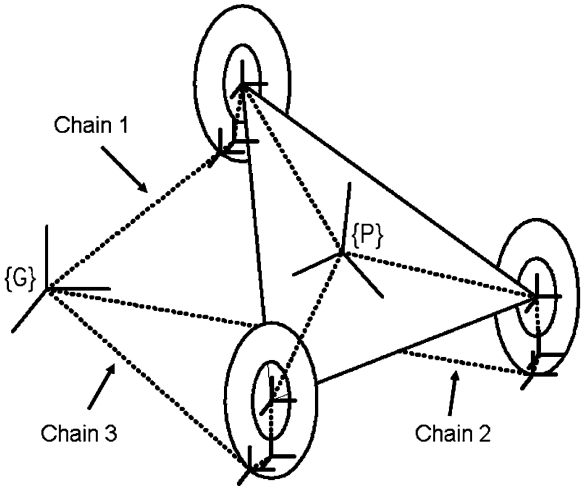

Fig. 16.7 Closure constraints: three kinematic chains in parallel must meet in frame $\{P\}$

robot are:

$$T_{GP,wheel1} = T_{GP,wheel2} = T_{GP,wheel3}. \tag{16.11}$$

These can be interpreted as ensuring that the robot platform remains rigid. Equation (16.11) can be written as

$$\begin{aligned} T_{GP,wheel1} - T_{GP,wheel2} &= 0 \\ T_{GP,wheel1} - T_{GP,wheel3} &= 0, \end{aligned} \tag{16.12}$$

which are algebraic equations of the form $C(q) = 0$. To avoid having to solve a set of differential and algebraic equations (DAEs), $C(q)$ is differentiated to obtain:

$$\dot{C}(q) = \frac{\partial C}{\partial q}\,\dot{q} = J(q)\,\dot{q}. \tag{16.13}$$

16.3.3.1 Constraint Stabilization

The Eq. (16.13) are velocity-level constraints, and during the simulation integration errors can accumulate leading to violation of the position-level constraints $C(q) = 0$. Many different algorithms have been proposed to deal with this well known issue in numerical integration of DAEs [22]. We choose a method based on the widely used Baumgarte stabilization method [23] used by Yun and Sarkar [24] because it is simple to implement, has a clear interpretation, and is effective for our simulation. In their approach, the authors suggests replacing (16.13) with:

$$J(q)\,\dot{q} + \sigma C(q) = 0, \quad \sigma > 0, \tag{16.14}$$

which for any arbitrary initial condition C_0 has the solution of the form $C(t) = C_0\, e^{-\sigma t}$. Since $\sigma > 0$, the solution converges exponentially to the desired constraints $C(q) = 0$ even if the constraints become violated at some point during the simulation. For our simulation, we found that values of σ between 1 and 10 produced good results ($\|C(q)\|_2 < 3 \times 10^{-4}\ \forall\, t$).

16.3.4 Definition of Platform Velocities

We are interested in the motion of the platform resulting from the input joint velocities $\dot{\theta}$. The time derivative of the coordinate transform relating the ground frame $\{\mathrm{G}\}$ and the platform frame $\{\mathrm{P}\}$ is

$$\dot{T}_{GP} = \begin{bmatrix} \dot{R}_{GP} & \dot{p}_{GP} \\ 0 & 0 \end{bmatrix}.$$

The linear velocity of the origin of the platform frame relative to the ground frame is $v_P = \dot{p}_{GP}$. The rotational velocity of the platform expressed in the platform frame is $\omega_P = \left(R_{GP}^T \dot{R}_{GP}\right)^\vee$, where the `vee` operator $\vee$ extracts the 3×1 vector components from the skew-symmetric matrix $R^T \dot{R}$ [17]. These output velocities are coupled in a 6×1 vector and are written as a linear combination of $\dot{\theta}$ and $\dot{\eta}$:

$$V_P = \begin{bmatrix} v_P \\ \omega_P \end{bmatrix} = \Phi_{V_P} \begin{bmatrix} \dot{\theta} \\ \dot{\eta} \end{bmatrix}. \tag{16.15}$$

These are the linear velocities of the platform frame in the global frame, and the angular velocities of the platform resolved in the local platform frame.

16.3.5 Forward Kinematics Equations

We now have all of the tools that we need to make a complete set of ordinary differential equations (ODEs) to model the robot/ground system. First, we collect the position and velocity variables of the system into vectors q and $\dot{q}$ as:

$$q = \begin{bmatrix} \theta \\ \eta \\ P_{PG} \\ \tilde{P}_c \end{bmatrix}, \quad \dot{q} = \begin{bmatrix} \dot{\theta} \\ \dot{\eta} \\ V_{PG} \\ \tilde{V}_c \end{bmatrix}, \tag{16.16}$$

where P_{PG} and $\tilde{P}_c$ are the position equivalents of V_{PG} and $\tilde{V}_c$, respectively.

Equation (16.10) relate the desired and actual joint velocities of the system. The rolling contact equation (16.4) are the non-holonomic system constraints. The stabilized holonomic constraints ensure that the wheels remain in the proper position and orientation relative to one another. The platform velocities are calculating according

to (16.15). As all of these ODEs are linear in the velocity terms, they can be collectively written in the form:

$$M(q)\,\dot{q} = f(q) \tag{16.17}$$

where

$$M(q)\,\dot{q} = \begin{bmatrix} I & 0 & 0 & 0 \\ -\Phi_{V_P 1} & -\Phi_{V_P 2} & I & 0 \\ J_1 & J_2 & J_3 & J_4 \\ 0 & I & 0 & -[CK] \end{bmatrix} \begin{bmatrix} \dot{\theta} \\ \dot{\eta} \\ V_{PG} \\ \tilde{V}_c \end{bmatrix},$$

$$f(q) = \begin{bmatrix} J_{in}\dot{\theta}_d \\ 0 \\ -\sigma\, C(q) \\ 0 \end{bmatrix},$$

where $\Phi_{V_P} = [\Phi_{V_P 1}\ \Phi_{V_P 2}]$ and $J(q) = [J_1\, J_2\, J_3\, J_4]$. The Eq. (16.17) completely describe the robot/ground system with inputs $\dot{\theta}_d$.

16.3.6 Adaptability of the Modeling Method

Our formulation is adaptable to other vehicle designs of arbitrary complexity: one simply has to create new coordinate transforms T_{GP} which reflect the geometry of the new system. All other equations will remain identical in structure to those presented here. This makes our modeling method versatile and powerful for realistic kinematic simulations of outdoor vehicles operating on rough terrains.

16.4 Results and Discussion

One of the advantages of our simulation is that it allows us to explore the motion of the wheeled mobile robot on uneven terrains of arbitrary shape. We ran the simulation on several different surfaces and for various inputs. `MATLAB`'s ODE suite was used to solve Eq. (16.17) and the Spline Toolbox was used to generate the ground surfaces. We present results for two surfaces: a high plateau and a randomly-generated hilly terrain.

16.4.1 Descending a Steep Hill

Here we present a simulation of the three-wheeled mobile robot descending from a high plateau down a steep hill. To the authors' knowledge, this simulation, which precisely models the rolling motion of the wheels on a complex ground surface, is not possible with other existing methods. Figure 16.8 shows the three-wheeled robot on the ground surface.

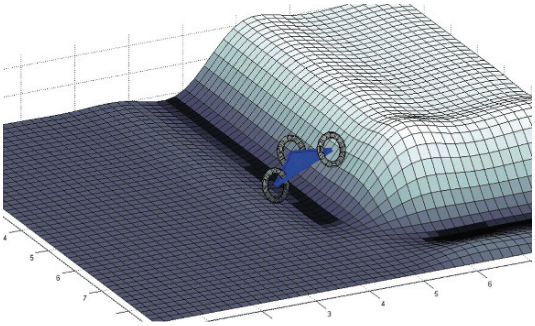

Fig. 16.8 The wheeled mobile robot on the plateau terrain

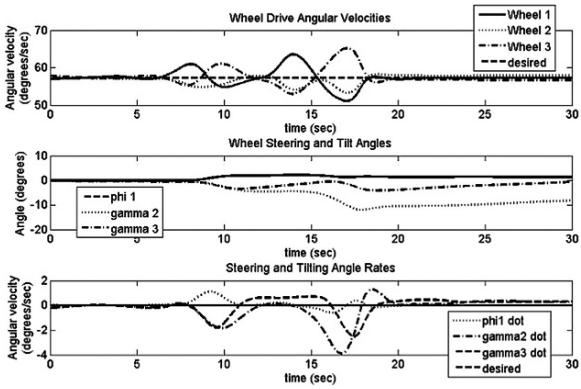

Fig. 16.9 Joint angles and rates: wheel drive rates, steering angle, and PVC angles

The simulation was run for 30 seconds with the following desired inputs:

- Steering rate $\dot{\phi}_1 = 0$
- Driving rates $\dot{\alpha}_{1,2,3} = 1\ rad/sec \approx 57.3\ deg/sec$
- PVC joint rates $\dot{\gamma}_{2,3} = 0$

Figure 16.9 plots the $\dot{\theta}$ inputs and the steering and PVC angles along with their desired values $\dot{\theta}_d$.

The platform velocities V_p are plotted in Fig. 16.10. Figure 16.11 plots the L_2 error in satisfaction of the holonomic constraint equations (16.12) and the rolling contact kinematic Eq. (16.4). Figure 16.11 shows that the constraint equations are well satisfied during the course of the simulation. This means that motion over the extreme terrain is possible with minimal wheel slip.

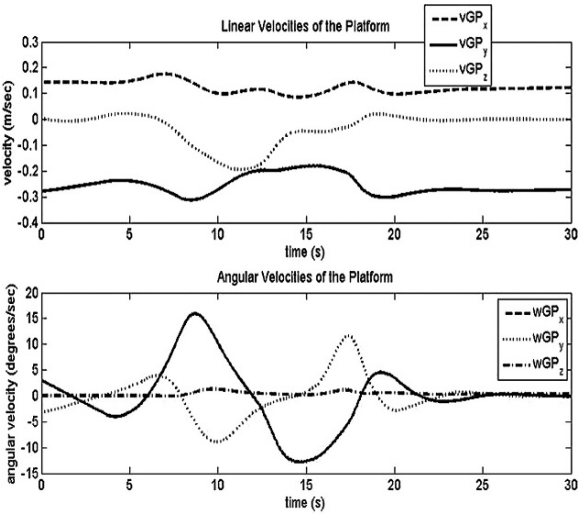

Fig. 16.10 The platform linear and angular velocities

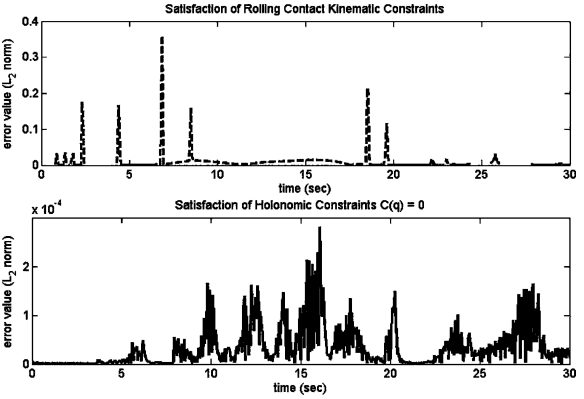

Fig. 16.11 The L_2 error in satisfaction of the holonomic and non-holonomic constraints

16.4.2 Random Terrain

Our simulation works for arbitrarily complex surfaces. Figure 16.12 shows the three-wheeled robot negotiating a randomly-generated ground surface. The inputs for this simulation were the same as for the plateau simulation in the previous section. Figure 16.13 plots the paths of the three wheel/ground contact points in the ground x-y plane. It also shows the projections of the wheel centers in that plane, to show that the wheels tilt as the robot traverses the uneven terrain. Figures 16.14 and 16.15 show the input joint velocities $\dot{\theta}$ and the output platform velocities V_p for the random terrain simulation.

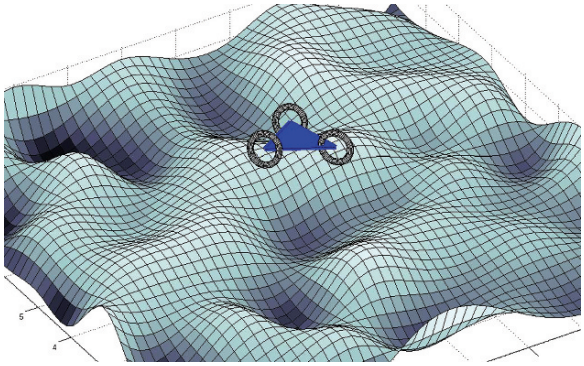

Fig. 16.12 The wheeled mobile robot on the random terrain

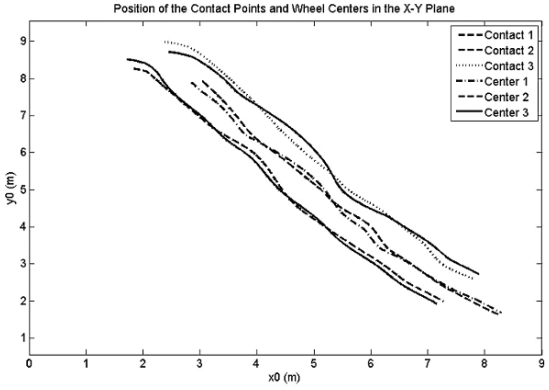

Fig. 16.13 The wheel/ground contact points and wheel centers in the xG-yG plane

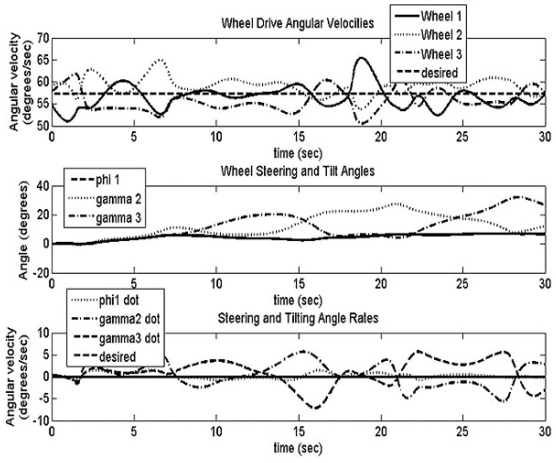

Fig. 16.14 Joint angles and rates: wheel drive rates, steering angle, and PVC angles

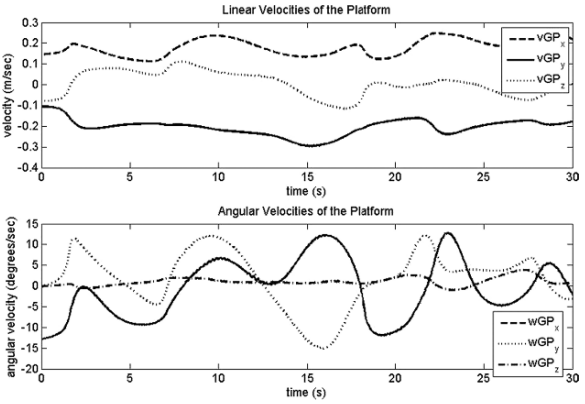

Fig. 16.15 The platform linear and angular velocities

16.5 Conclusion and Future Work

We have described a novel kinematic simulation of a three-wheeled mobile robot equipped with Passive Variable Camber (PVC) and moving on uneven terrain. PVC adds an extra degree of freedom at each wheel/platform joint, thereby allowing the wheel to tilt laterally. This extra motion allows the vehicle to better adapt to uneven terrain and reduce wheel slip, which is harmful to vehicle efficiency and performance.

Making use of concepts adapted from dextrous manipulator kinematics, our technique produces a model governed by a manageable set of linear ODEs. The resulting equations can tell us the instantaneous mobility (number of degrees of freedom) of the robot/ground system. We also showed a way of specifying joint velocity inputs which are compatible with system constraints. This could be useful on a real system in order to control the vehicle to minimize wheel slip. Our modeling technique is adaptable to vehicles of arbitrary number of wheels and joints.

Based on our simulation results, PVC has the potential to greatly improve the motion performance of wheeled mobile robots or any wheeled vehicle which moves outdoors on rough terrain by reducing wheel slip.

We are currently working on a number of extensions to this work. Under development is a way to do path planning for the PVC-equipped mobile robot. Our simulation will be used to verify that the robot can navigate from an initial position to any final configuration without wheel slip. Also, the kinematic model provides an excellent intermediate step to a full dynamic simulation. With a suitable friction model, the equations governing the wheel/ground contact kinematics can be easily extended to sliding contact. This could enhance the simulation by allowing a comparison between a vehicle with PVC and one without. PVC's effects on power consumption and localization ability will be explored in future versions of the simulation.

We are also designing and building a test set-up with a PVC-equipped wheel rolling on an uneven surface. The wheel will be instrumented to measure slip so that the efficacy of PVC for reducing wheel slip can be studied.

References

1. Alexander, J.C. and Maddocks, J.H. 1989. "On the Kinematics of Wheeled Mobile Robots". *J. Robot. Res.*, Vol. 8, No. 5, pp. 15–7.
2. Iagnemma, K., Golda, D., Spenko, M., and Dubowsky, S. 2003. "Experimental Study of High-speed Rough-terrain Mobile Robot Models for Reactive Behaviors". *Springer Tr. Adv. Robot*., Vol. 5, pp. 654–663.
3. Lacaze, A., Murphy, K., and DelGiorno, M. 2002. "Autonomous Mobility for the DEMO III Experimental Unmanned Vehicles". *Proc. AUVSI 2002*, Orlando, FL.
4. Waldron, K. 1994. "Terrain Adaptive Vehicles". *ASME J. Mechanical Design*, Vol. 117, pp. 107–112.
5. Choi, B. and Sreenivasan, S. 1998. "Motion Planning of a Wheeled Mobile Robot with Slip-Free Motion Capability on a Smooth Uneven Surface". *Proc. 1998 IEEE ICRA*.
6. Divelbiss, A. and Wen, J. 1997. "A Path Space Approach to Nonholonomic Motion Planning in the Presence of Obstacles". *IEEE Trans. Robot. Automat.*, Vol. 13, No. 3, pp. 443–451.
7. Tarokh, M., McDermott, G., Hiyati, S., and Hung, J. 1999. "Kinematic Modeling of a High Mobility Mars Rover". *Proc. 1999 IEEE International Conference on Robotics and Automation*, May 10–15, 1999, Detroit, Michigan, USA.
8. Meghdari, A., Mahboobi, S., and Gaskarimahalle, A. 2004. "Dynamics Modeling of "Cedra" Rescue Robot on Uneven Terrains". *Proc. IMECE 2004*.
9. Tai, M. 2003. "Modeling of Wheeled Mobile Robot on Rough Terrain". *Proc. IMECE2003*.
10. Grand, C., BenAmar, F., Plumet, F., and Bidaud, P. 2004. "Decoupled Control of Posture and Trajectory of the Hybrid Wheel-Legged Robot Hylos". *Proc. 2004 IEEE International Conference on Robotics and Automation*, ICRA 2004, April 26–May 1, 2004, New Orleans, LA, USA.
11. Sreenivasan, S.V. and Nanua, P. 1999. "Kinematic Geometry of Wheeled Vehicle Systems". *Trans. ASME J. Mech. Des.*, Vol. 121, pp. 50–56.
12. Chakraborty, N. and Ghosal, A. 2004. "Kinematics of Wheeled Mobile Robots on Uneven Terrain". *Mech. Mach. Theor*. Vol. 39, No. 12, pp. 1273–1287.
13. Choi, B., Sreenivasan, S., and Davis, P. 1999. "Two Wheels Connected by an Unactuated Variable Length Axle on Uneven Ground: Kinematic Modeling and Experiments". *ASME J. of Mech. Des*., Vol. 121, pp. 235–240.
14. Huntsberger, T., Aghazarian, H., Cheng, Y., Baumgartner, E., Tunstel, E., Leger, C., Trebi-Ollennu, A., and Schenker, P. 2002. "Rover Autonomy for Long Range Navigation and Science Data Acquisition on Planetary Surfaces". *Proc. 2002 IEEE ICRA*.
15. Lamon, P. and Siegwart, R. 2006. "3D Position Tracking in Challenging Terrain". *International Conference on Field and Service Robotics*, July 2007, Chamonix, France, STAR 25, pp. 529–540.
16. Montana, D. 1988. "The Kinematics of Contact and Grasp". *International Journal of Robotics Research*, Vol. 7, No. 3, pp. 17–32.
17. Murray, R., Li, Z., and Sastry, S. 1994. *A Mathematical Introduction to Robotic Manipulation.* CRC Press: Boca Raton, FL.
18. Montana, D. 1995. "The Kinematics of Multi-Fingered Manipulation". *IEEE Trans. Robot. Automat.*, Vol. 11, No. 4, pp. 491–503.
19. Han, L. and Trinkle, J.C. 1998. "The Instantaneous Kinematics of Manipulation". *Proc. 1998 IEEE ICRA*, pp. 1944–1949.

20. Kim, S.S. and Vanderploeg, M.J. 1986. “QR Decomposition for State Space Representation of Constrained Mechanical Dynamic Systems”. *J. Mech. Trans. Automat. Des*., Vol. 108, pp. 183–188.
21. Nash, J.C. 1990. *Compact Numerical Methods for Computers*. Second edition. Adam Hilger Publishing: Bristol.
22. Laulusa, A. and Bauchau, O.A. 2007. “Review of Classical Approaches for Constraint Enforcement in Multibody Systems”. *Journal of Computational and Nonlinear Dynamics*, submitted for publication.
23. Baumgarte, J. 1983. “A New Method of Stabilization for Holonomic Constraints”. *ASME Journal of Applied Mechanics*, Vol. 50, pp. 869–870.
24. Yun, X. and Sarkar, N. 1998. “Unified Formulation of Robotic Systems with Holonomic and Nonholonomic Constraints”. *IEEE Trans. Robot. Automat*., Vol. 14 No. 4, pp. 640–650.